Journal of Alloys and Compounds 509S (2011) S640–S645

Contents lists available at ScienceDirect

Journal of Alloys and Compounds

journal homepage: www.elsevier.com/locate/jallcom

Microstructural evolution and improved hydrogenation–dehydrogenation kinetics of nanostructured melt-spun Mg–Ni–Mm alloys

Y. Wu[a,b,c,*], M.V. Lototsky[d,e], J.K. Solberg[c], V.A. Yartys[c,d]

[a] School of Materials Science and Engineering, Shanghai Institute of Technology, No. 120, Cao Bao Road, Shanghai 200235, PR China
[b] China Iron & Steel Research Institute Group, Advanced Technology & Materials Co., Ltd., No. 76 Xueyuan Nanlu, Haidian, Beijing 100081, PR China
[c] Department of Materials Technology, Norwegian University of Science and Technology, NO-7491 Trondheim, Norway
[d] Institute for Energy Technology, P.O. Box 40, N-2027 Kjeller, Norway
[e] University of the Western Cape, South Africa

ARTICLE INFO

Article history:
Received 21 July 2010
Received in revised form
22 November 2010
Accepted 22 November 2010
Available online 30 November 2010

Keywords:
Hydrogen absorbing materials
Rapid solidification
Microstructure
Transmission electron microscopy

ABSTRACT

The microstructural evolution of as-quenched ribbons and ball-milled hydrides of the Mg–10Ni–2Mm alloy was studied by TEM. These studies showed a refinement of the microstructures during the applied processing and a nucleation of $MmMg_{12}$ intermetallic at the grain boundaries of Mg and Mg_2Ni. The interface between $MmMg_{12}$ and Mg_2Ni is semi-coherent, with an ordered repetition of the consistent atomic arrangements. The kinetics of H-absorption/desorption is improved due to the fast hydrogen diffusion in the nanograins, thus, providing paths for H-exchange. TEM studies showed (a) stability of the nano-sized grains in the ball-milled Cu-1000 (the surface velocity of the copper wheel: 1000 rpm) sample that underwent cycling of hydrogen desorption and absorption during heating to 350 °C; (b) formation of MmH_{3-x} hydride from $MmMg_{12}$ and its preferential location at grain boundaries of MgH_2. Clearly, MmH_{3-x} and Mg_2NiH_4 act as nucleation centres to initiate the formation of MgH_2, thus, promoting hydrogen absorption by the Mg alloys. Pressure–composition–temperature diagrams show the presence of two plateaux, Mg–MgH_2 and Mg_2Ni–Mg_2NiH_4. The MgH_2 plateau showed no hysteresis and practically no slope, while the plateau for Mg_2NiH_4 exhibited both a pronounced hysteresis and a slope, particularly for the nanocrystalline sample. The maximum hydrogen storage capacity of the nanocrystalline sample was higher than that of the microcrystalline one.

1. Introduction

Magnesium is an attractive material for hydrogen storage applications benefiting from high hydrogen storage capacity, low density, and rich natural resources. However, slow hydrogenation kinetics and high dehydriding temperatures limit its actual use [1]. The reaction kinetics of Mg with H_2 is improved by additives of transition and rare earth metal elements such as Ni, Ti, V, La, Nd and Y [2]. In our earlier study, we have observed that hydrogen absorption/desorption rates in Mg-based alloys are dramatically enhanced by nanoprocessing [3–6]. The rapid solidification (RS) technique is an efficient process in improving the hydrogen storage properties of Mg-based alloys by obtaining nanocrystalline microstructures. The large number of interfaces and grain boundaries available in the nanocrystalline materials provide easy pathways for hydrogen diffusion and promote the absorption of hydrogen. Reactive Ball Milling in hydrogen is well-known as an efficient method for synthesis of Mg-based hydrides [7].

In the present study, microcrystalline and nanocrystalline microstructures of Mg–10Ni–2Mm (at.%) alloy were synthesised by applying a single roller melt-spinning technique followed by a ball-milling process to obtain the hydrides. The microstructural evolution of the melt-spun ribbons and hydrides after the temperature desorption spectroscopy (TDS)–hydrogenation cycling was studied, and the hydrogenation–dehydrogenation behavior was investigated by PCT (pressure–composition–temperature) and TDS methods focusing on the effect of nanostructuring on the hydrogen storage properties.

2. Experimental

The as-cast Mg–10Ni–2Mm (at.%) alloy was prepared by a two-step method of pre-alloying and vacuum induction melting of a mixture of 99.7% lanthanum-rich Mischmetal, 99.98% pure magnesium and 99.98% pure nickel. The melt-spun ribbons were obtained by a single roller melt-spinning technique (copper quenching disc with a diameter of 200 mm) in an argon atmosphere of 200 mbar. The details are described elsewhere [3–5]. The surface velocity of the copper wheel was from 3.1 (300 rpm) or 10.5 m s^{-1} (1000 rpm), and the corresponding melt-spun ribbon

* Corresponding author at: School of Materials Science and Engineering, Shanghai Institute of Technology, No. 120, Cao Bao Road, Shanghai, 200235, P.R. China. Tel.: +86 10 64941773; fax: +86 10 64941773.
E-mail address: science2008@live.cn (Y. Wu).

0925-8388/$ – see front matter © 2010 Elsevier B.V. All rights reserved.
doi:10.1016/j.jallcom.2010.11.140

Table 1
The reference data for the constituent phases in the as-cast Mg–10Ni–2Mm alloy [8].

Sample	Constituent phases								
	Mg			Mg_2Ni			$MmMg_{12}$		
	Space group	Lattice periods (Å)	Abundance (wt.%)	Space group	Lattice periods (Å)	Abundance (wt.%)	Space group	Lattice periods (Å)	Abundance (wt.%)
As-cast	$P6_3/mmc$	$a = 3.20840(9)$ $c = 5.2078(2)$	48.9(2)	$P6_222$	$a = 5.2111(2)$ $c = 13.2491(3)$	35.8(2)	$I4/mmm$	$a = 10.315(3)$ $c = 5.952(2)$	15.2(1)

samples are labelled Cu-300 and Cu-1000, respectively. Prior to the dehydrogenation, the as-quenched ribbons were ball-milled in hydrogen at a pressure of 30 bar in order to synthesise corresponding hydrides. Reactive Ball Milling was carried out in a vial with a rotation speed of 500 rpm, using the planetary mill "FRITCH Pulverisette 6" planetary mill. The ball-to-powder ratio was 80:1.

The reaction kinetics was studied by the Sieverts method, by measuring the pressure change in a closed system with a constant volume. TDS (thermal desorption spectroscopy) of hydrogenated samples was conducted in a conventional Sieverts-type apparatus to determine the onset temperature of hydrogen release during dehydrogenation. Several cycles of hydrogenation–TDS were performed for each sample. The hydrogen storage capacities and equilibrium diagrams of hydrogen absorption and desorption were measured by studying the PCT isotherms. The midpoints of the pressure plateaux of the PCT curves were taken as the data for building the van't Hoff plots.

The structure, composition and morphology of the phases of the hydrogenated and dehydrogenated samples were examined by X-ray diffractometry (XRD) and transmission electron microscopy (TEM, JEM-2010) equipped with an energy-dispersive X-ray spectrometer (EDS).

3. Results and discussion

As reported in our previous publications [3–5], the as-cast Mg–10Mm–2Ni alloy is a ternary eutectic alloy with two intermetallic phases present, Mg_2Ni and $MmMg_{12}$, embedded into a matrix of pure Mg. It is inhomogeneous with prevailing areas of a coarse microstructure and much smaller areas of a very fine microstructure. The reference data for the constituent phases are listed in Table 1 [8]. The grain size was greatly reduced by applying the RS processing. Fig. 1 shows HREM micrographs of the melt-spun ribbons that were rapidly solidified at a wheel surface velocity of 3.1 m s^{-1}. Three phases, namely, Mg, Mg_2Ni and $MmMg_{12}$, were identified. As shown in Fig. 1(a), the nano-sized Mg_2Ni rods (length approximately 100 nm) nucleated in the matrix of Mg grains. The average size of the equiaxed Mg particles was determined to be approximately 500 nm. Fig. 1(b) shows a typical $MmMg_{12}$ particle with a size of approximately 400 nm and its corresponding [7 5 3] zone axis SADP (selected area diffraction pattern). It is clear that the $MmMg_{12}$ intermetallic alloy preferably nucleates at the boundaries of the Mg grains. The Mg_2Ni precipitates shown in Fig. 1 have an average size of 10 nm × 200 nm. Long interface boundaries between the Mg_2Ni and Mg phases, and formation of the Mm-rich intermetallic promotes fast hydrogen diffusion through the samples.

The nanocrystalline microstructure consisting of nanostructured Mg and Mg_2Ni was obtained when the surface velocity of the copper wheel increased to 10.5 m s^{-1}. Fig. 2 shows HREM micrographs of the interface between Mg_2Ni and $MmMg_{12}$ inserted their corresponding [3 6 2] and [8 3 1] zone axis SADPs, and between Mg and $MmMg_{12}$ in the melt-spun Mg–10Ni–2Mm alloy. As expected, in a multi-phase Mg alloy, the phases with the lower concentration of magnesium (Mg_2Ni and $MmMg_{12}$) are surrounded by the Mg metal. Due to the large difference of the interplanar distances between the Mg_2Ni and $MmMg_{12}$ at the interface, it produces some dislocations to reduce the interfacial elastic strain energy. Consequently, part of the interface atoms maintain the two-phase matching, thus creating a semi-coherent interface between Mg_2Ni and $MmMg_{12}$, which is shown in Fig. 2(a). The Fig. 2(a) also demonstrates a certain degree of mismatch between the atomic arrangements in these phases. Thus, higher energy sites are easily formed and become nucleation centres for the hydrides at the interface. In turn, a formation of non-coherent interface was observed between $MmMg_{12}$ and Mg, due to a big difference in crystallographic characteristics between these two phases, see Fig. 2(b). Such an interface can also act as hydride nucleation sites due to its higher energy as compared to the volume inside grains, and, furthermore, high hydrogen affinity of the $MmMg_{12}$ resulting in its preferential hydrogenation. The large area of non-

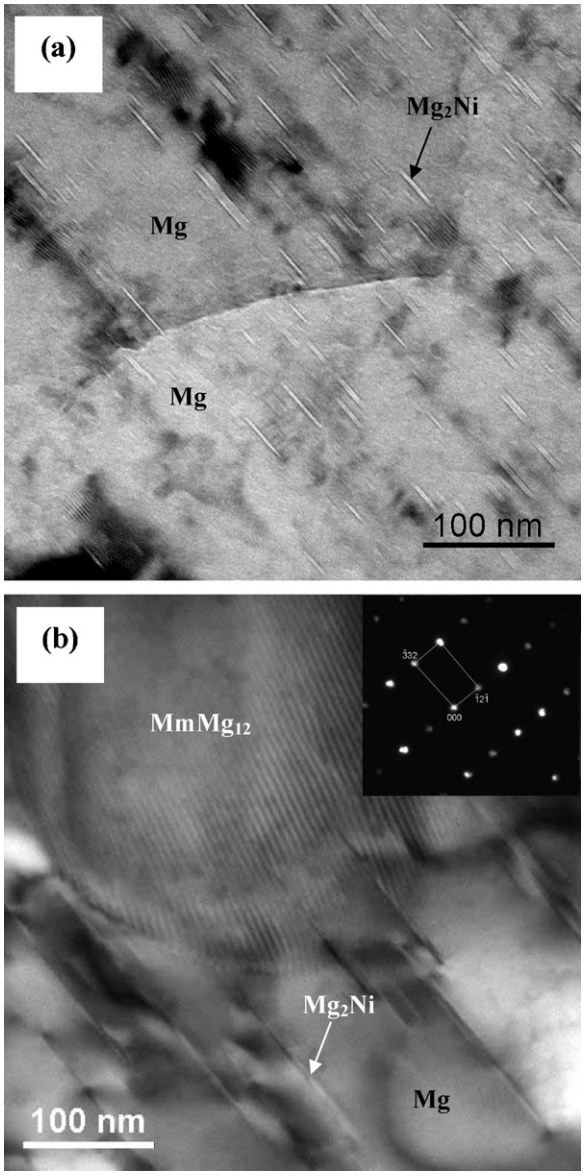

Fig. 1. HREM micrographs showing: (a) the nano-sized Mg_2Ni nucleation in the matrix of Mg grains, and (b) a coarse $MmMg_{12}$ grain at the boundary of Mg and its corresponding [7 5 3] zone axis SADP in the melt-spun Mg–10Ni–2Mm solidified with a copper wheel surface velocity of 3.1 m s^{-1}.

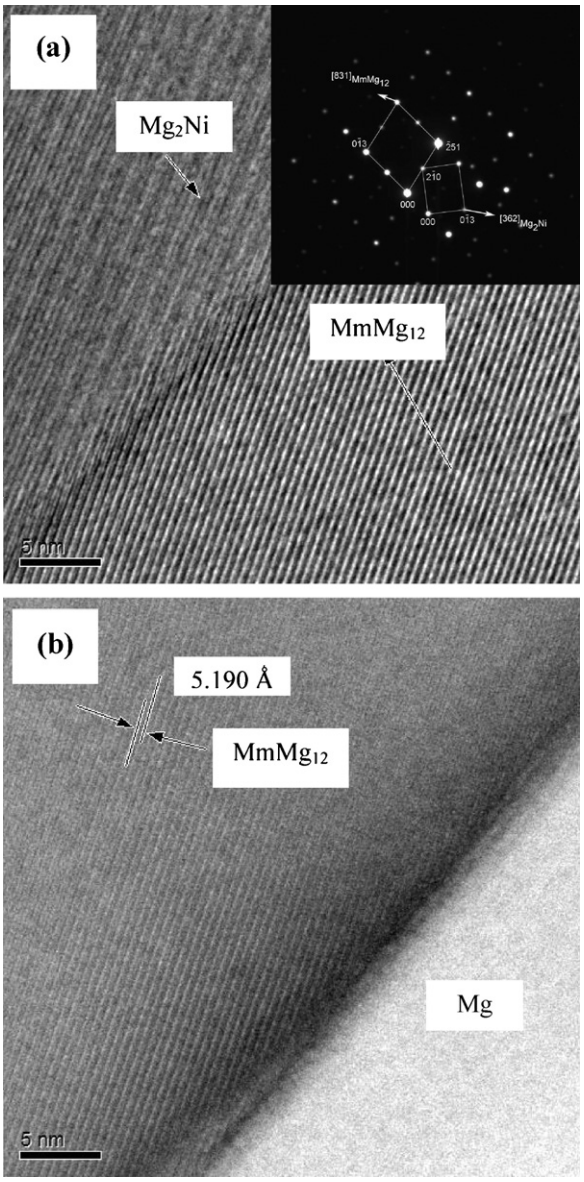

Fig. 2. HREM micrographs showing: (a) the semi-coherent relationship between Mg_2Ni and $MmMg_{12}$ inserted their corresponding [3 6 2] and [8 3 1] zone axis SADPs and (b) the interface between Mg and $MmMg_{12}$ in the melt-spun Mg–10Ni–2Mm alloy solidified with a copper wheel surface velocity of 10.5 m s^{-1}. The shown (2 0 0) interplanar distance of $MmMg_{12}$ is 5.190 Å.

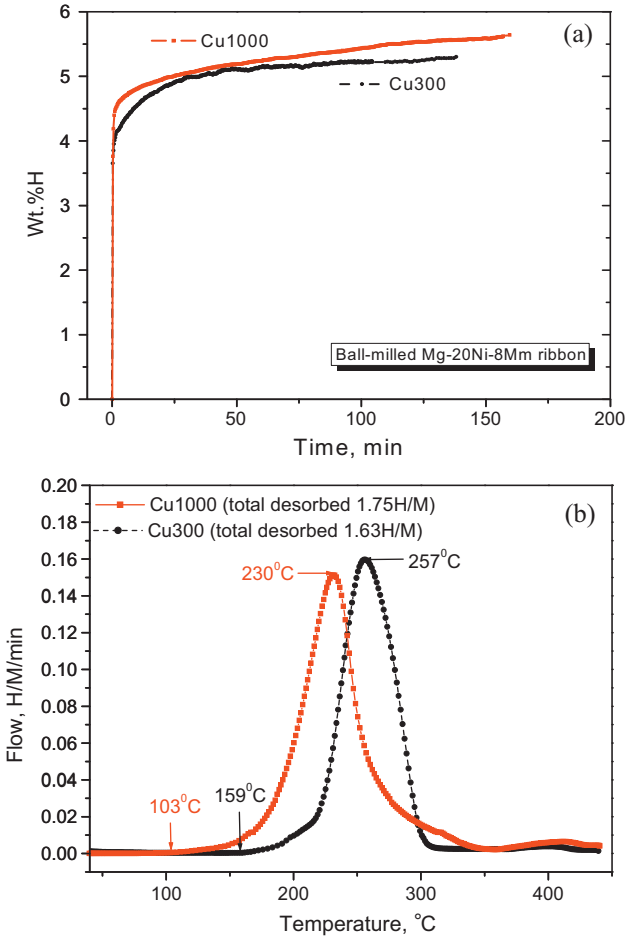

Fig. 3. Comparison of hydrogen storage properties of the ball-milled Mg–10Ni–2Mm ribbons solidified with copper wheel surface velocities of 3.1 and 10.5 m s^{-1}: (a) the 2nd cycle hydrogenation curves at $T = 300\,^{\circ}C$ and $P_{H_2} = 30$ bar, and (b) the 2nd cycle TDS curves of hydrogen thermal desorption in vacuum (heating rate 5 °C/min) from the hydrogenated alloy.

coherent interface between $MmMg_{12}$ and Mg is reduced by the formation of the semi-coherent interfaces between $MmMg_{12}$ and Mg_2Ni, improving the hydrogenation performance. Because the lattice deformation due to hydrogenation is decreased for the latter phases, the pressure hysteresis of H-absorption/desorption is expected to be diminished.

In order to obtain the hydrides, the melt-spun ribbons were ball-milled under the hydrogen atmosphere at a pressure of 30 bar. For both RS synthesised samples, irrespective of their microstructure, the hydrogenation resulted in the formation of MgH_2, Mg_2NiH_4 and Mm-based hydrides. The latter hydride was formed during decomposition of $MmMg_{12}$ to form MmH_{3-x} and MgH_2. The kinetics of the H-absorption reaction for the ball-milled melt-spun ribbons was further improved following an increase in the cooling rate during solidification. Fig. 3(a) shows typical data of hydrogen absorption by the ball-milled melt-spun samples collected at 300 °C. Repeated hydrogenations after completing the thermal desorption from the synthesised hydrides resulted in an improvement of the hydrogen absorption kinetics. The dynamics of H-absorption became reproducible after the 3rd cycle for the ball-milled Cu-1000 sample and after the 5th cycle for the ball-milled Cu-300 sample. Both samples absorbed hydrogen very fast, and it took less than 60 s to reach H absorption capacity exceeding 4 wt.% H. The saturated hydrogen storage capacity for the ball-milled Cu-300 and Cu-1000 samples was 5.3 and 5.6 wt.% H, respectively. Thus, the ball-milled Cu-1000 alloy showed better kinetic performance and higher maximal hydrogen absorption capacity. The improved kinetics is a result of the microstructural refinement, while the hydrogen absorption capacity is determined by the completeness of hydrogenation of the different hydride phases, particularly important in case of the formation of MgH_2. Compared with the ball-milled Cu-1000 sample, a small decrease in the hydrogen absorption kinetics was observed for the Cu-300 sample after several cycles, which is due to the formation of the coarse heterogeneous grains after the RS synthesis. Although the microstructure of Cu-300 was greatly refined after the ball-milling, the nanostructuring was less developed as compared to the sample Cu-1000.

TDS measurements were performed using a heating rate of 0.5 °C/min. The H-desorption temperature of the ball-milled materials was lowered. Typical TDS spectra for the hydrogenated ball-milled samples are presented in Fig. 3(b). For the Cu-300-based hydride, the desorption took place in a broad temperature interval between 160 and 300 °C with a peak around 257 °C. A pro-

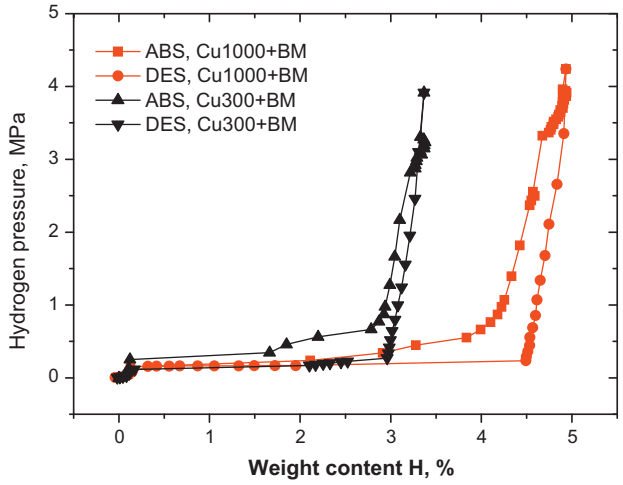

Fig. 4. PCT absorption and desorption isotherms for the ball-milled Mg–10Ni–2Mm ribbons at 300 °C.

nounced lowering of the desorption temperatures takes place for the ball-milled Cu-1000-based hydride. The desorption proceeds in a temperature range between ~100 and 350 °C, with a peak at ~230 °C. We conclude that the remarkable lowering of the hydrogen desorption temperature achieved for the Mg–10Ni–2Mm alloy is caused by catalytic effects of Ni and Mm on the desorption process and by the formation of a uniform nano-sized microstructure in the Cu-1000 sample synthesised by RS and further modified by Reactive Ball Milling in hydrogen.

PCT diagrams measured for the ball-milled melt-spun samples are shown in Fig. 4. Two plateaux are visible; the lower plateau corresponds to the transformation $Mg \leftrightarrow MgH_2$, and the upper plateau belongs to the transformation $Mg_2Ni \leftrightarrow Mg_2NiH_4$ [9]. Ball-milling treatment normally increases plateau slope and hysteresis for the Mg_2Ni-based hydrides [10]. Thus, both these features are expected in the second hydrogen absorption–desorption plateau corresponding to the Mg_2Ni–Mg_2NiH_4 transformation. The values of ΔH and ΔS of Mg_2NiH_4 for the ball-milled Cu-300 and Cu-1000 samples are −73.7 kJ/mol H_2, −134.7 J/mol, and −65.9 kJ/mol H_2, −121.5 J/mol, respectively, which are in a fairly good agreement with the values of −67.5 kJ/mol H_2 and −124.4 J/mol for the as-cast alloy. The values of the formation enthalpy of MgH_2 in both ball-milled samples are consistent with those for the as-cast one. The hydrogen storage capacity of the ball-milled Cu-300 and Cu-1000 samples is 3.36 and 4.94 wt.% H, respectively. The lowering of the H capacity for the Cu-300 sample is because of the difficulties in achieving the hydrogenation of the part of the sample, as some of the small hard pieces of the melt-spun ribbons remained unactivated during the Reactive Ball Milling.

As shown in Fig. 5, the XRD patterns obtained from the different hydrogenated samples after several H-absorption cycles were rather similar to each other. However, the content of individual hydrides differed in the samples, reflecting the changes in their hydrogen storage capacities. As seen in Table 2, five different hydride phases, i.e. MgH_2, $Mg_2NiH_{0.3}$, high-temperature (HT) Mg_2NiH_4, low-temperature (LT) Mg_2NiH_4 and MmH_3 were identified. From the refinements, the weight content of these hydrides in the ball-milled Cu-300 and Cu-1000 materials was determined to be about 58, 14, 14, 8, 6 wt.%, and 60, 9, 16, 8, 7 wt.%, respectively. We note that the content of $Mg_2NiH_{0.3}$ in the latter material is much lower as compared to the former one, indicating a significantly deeper degree of hydrogenation of Mg_2Ni in the ball-milled Cu-1000 sample. It has been reported [11] that during the heating of the $Mg_{67}Ni_{28}Pd_5$, crystalline Mg_2Ni is formed at about 182 °C followed by the formation of crystalline Mg_2NiH_4 at about 247 °C. The

Table 2
Summary of the refinement of the XRD data of the hydrogenated Mg–10Ni–2Mm alloy.

Sample	Constituent phases														
	MgH_2			$Mg_2NiH_{-0.3}$			HT-Mg_2NiH_4			LT-Mg_2NiH_4			MmH_3		
	Space group	Lattice periods (Å)	Abundance (wt.%)	Space group	Lattice periods (Å)	Abundance (wt.%)	Space group	Lattice periods (Å)	Abundance (wt.%)	Space group	Lattice periods (Å)	Abundance (wt.%)	Space group	Lattice periods (Å)	Abundance (wt.%)
Cu-300	$P4_2/mnm$	$a = 4.5067(3)$ $c = 3.0171(4)$	57.9(2)	$P6_222$	$a = 5.240(3)$ $c = 13.36(2)$	14.0(4)	$Fm\bar{3}m$	$a = 6.458(1)$	13.9(2)	C2/c	$a = 14.57(1)$ $b = 6.394(5)$ $a = 14.31(2)$ $b = 6.294(5)$	8.4(3)	$Fm\bar{3}m$	$a = 5.545(2)$	5.8(1)
Cu-1000		$a = 4.5094(3)$ $c = 3.0168(3)$	59.6(2)		$a = 5.231(1)$ $c = 13.313(9)$	9.4(3)		$a = 6.4656(9)$	15.8(2)			7.8(4)		$a = 5.549(2)$	7.2(1)

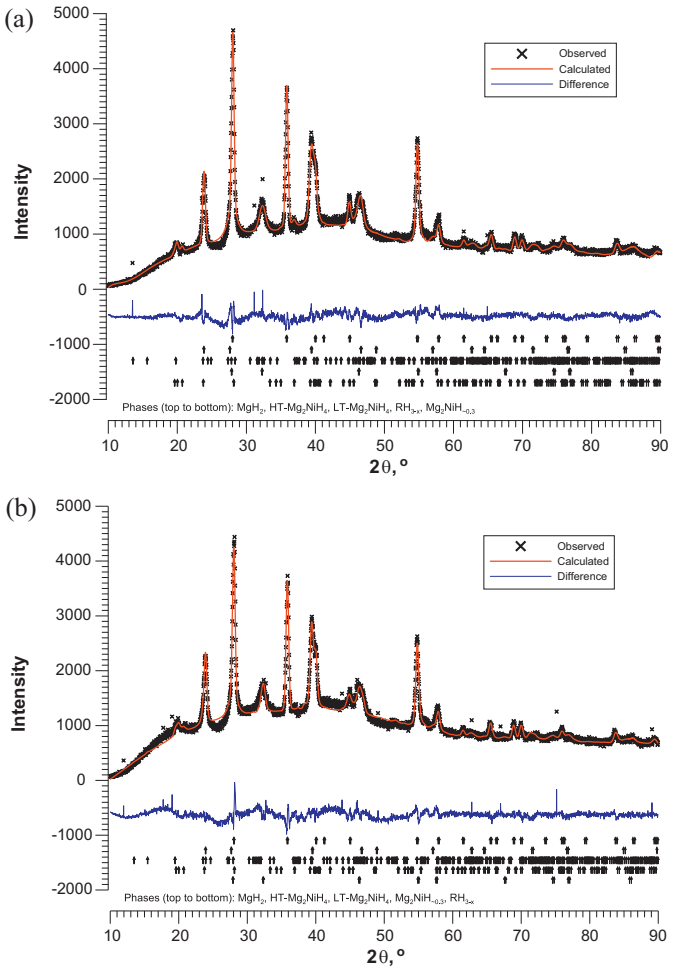

Fig. 5. XRD pattern of the ball-milled Mg–10Ni–2Mm ribbons: (a) Cu-300 sample hydrogenated in 30 bar H_2 for 2 h, and then 4 cycles of TDS/hydrogenation, and (b) Cu-1000 sample hydrogenated in 30 bar H_2 for 2 h, and then 3 cycles of TDS/hydrogenation.

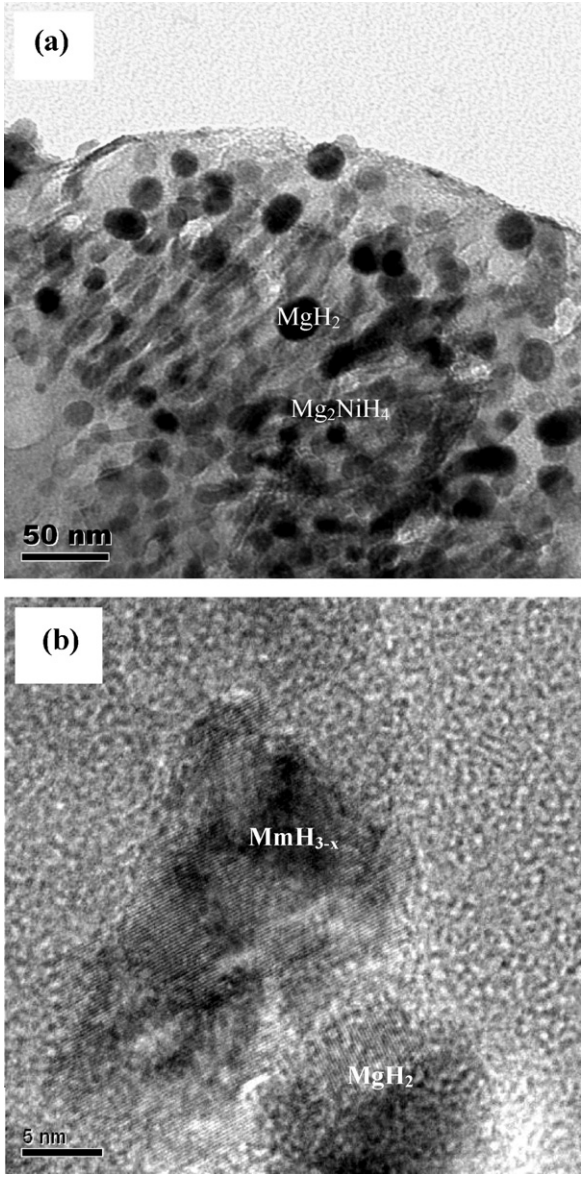

Fig. 6. TEM micrographs showing the microstructures of the ball-milled Cu-1000 Mg–10Ni–2Mm ribbon initially hydrogenated at 30 bar H_2 for 2 h, and went through the 3 cycles of hydrogen desorption–hydrogenation: (a) overall morphology of the nanocrystalline grains, and (b) MmH_{3-x} phase at the grain boundary of the MgH_2.

XRD data of the ball-milled Cu-300 sample (Fig. 5(a)) showed somewhat reduced intensities and line broadening, indicating smaller crystallite sizes as compared with the melt-spun Cu-300 sample in [3]. In contrast with the hydrogenated melt-spun alloy (where Mg_2NiH_4 was mainly present in its high-temperature (HT) cubic modification [3]), the hydrogenated ball-milled melt-spun samples contained both HT-Mg_2NiH_4 and LT-Mg_2NiH_4, further to an α-solid solution of hydrogen in Mg_2Ni, $Mg_2NiH_{0.3}$. The latter phase was present due to both incomplete hydrogenation of the samples and a partial hydrogen release from Mg_2NiH_4 during handling of the hydrogenated materials. In an earlier paper [4], the hydrogenated as-cast Mg–Ni–Mm alloy was reported to contain the hydrides MgH_2, LT-Mg_2NiH_4, HT-Mg_2NiH_4 and MmH_3, and the transition temperature between LT- and HT-Mg_2NiH_4 was about 230 °C. An increased amount of the cubic HT-Mg_2NiH_4 formed in our present experiments already at room temperature can be induced by ball milling causing severe mechanical stresses in the material and promoting the LT–HT phase transition [12].

The grain size of the Cu-300 sample was greatly reduced by the ball-milling; nanocrystalline grains were obtained in a part of a nonuniform matrix of Mg. After several cycles of the hydride decomposition–hydrogenation, the sample still contained coarse and fine grain areas; however, some slight grain growth occurred. The TEM micrographs in Fig. 6 show hydrogenated microstructures of the ball-milled Cu-1000 sample after 3 desorption–absorption cycles. Nano-sized grains consisting of the hydrides MgH_2, $Mg_2NiH_{0.3}$, Mg_2NiH_4 and MmH_{3-x} were found after the TDS processing of the sample at 350 °C. The rod-shaped Mg_2Ni-type hydrides and a considerable amount of nanocrystalline equiaxed MgH_2 particles of approximately 20 nm in size were formed, see Fig. 6(a). We note that the rod-shaped Mg_2Ni-type hydrides were distorted, thus, indicating high mechanical stresses caused by the Reactive Ball Milling processing followed by the subsequent TDS–hydrogenation cycles. Importantly, the grains remained nano-sized in the ball-milled Cu-1000 sample after 3 hydrogenation cycles, which assured presence of the paths for the fast diffusion of hydrogen. The presence of the secondary phases containing Mm and Ni and acting as nucleation centres for the formation of the nanostructured MgH_2 and catalysing hydrogen uptake, could explain beneficial properties of the RS alloys processed by the RBM. In the ball-milled Cu-1000 sample, some amorphous Mm-rich phases were observed. After hydrogenation, the crystallization occurred. Fig. 6(b) shows a HREM image of

the morphology of the MmH_{3-x} hydride located at the boundary of a MgH_2 particle, the MgH_2 phase mostly being wrapped in the MmH_{3-x} phase. An atomic arrangement within the MmH_{3-x} grain suggests that hydrogen absorption initiates the crystallization process of amorphous phases. Defects present within the amorphous phases are the nucleation centres for the crystallization of the nanocrystalline hydrides. These changes explain significant improvement of the hydrogenation properties.

4. Conclusions

1. The Mg–10Ni–2Mm (at.%) alloy processed by rapid solidification (at 300 and 1000 rpm) followed by a Reactive Ball Milling in hydrogen gas, yielded nanostructured hydrides of Mg, Mg_2Ni and Mm (the latter was formed during a disproportionation of the tetragonal intermetallic compound $MmMg_{12}$). During the solidification, the $MmMg_{12}$ compound nucleates at the grain boundaries of Mg and Mg_2Ni. It preferentially absorbs hydrogen during the hydrogenation, thus, providing H-conducting paths for the fast hydrogen exchange. An ordered repetition of the atomic arrangements formed the semi-coherent interface between $MmMg_{12}$ and Mg_2Ni. In contrast, a non-coherent structure was formed at the interface of $MmMg_{12}$ and Mg and was identified as a precursor for the nucleation of the hydrides.
2. During the dehydrogenation–hydrogenation cycling, the nanosized grains in the ball-milled Cu-1000 sample remain rather stable, thus yielding the microstructural stability. MmH_{3-x} and Mg_2NiH_4 act as nucleation centres for the formation of MgH_2, promoting hydrogen absorption by the Mg alloys.
3. The kinetics of hydrogen absorption/desorption is greatly improved by the refined microstructures, due to the fast hydrogen diffusion in the nanograins. The maximum hydrogen storage capacity of the ball-milled Cu-1000 sample is higher than that of the Cu-300 one. A pronounced shift of the thermal stability takes place for the Cu-1000 sample as compared to Cu-300.

Acknowledgments

The work presented in this paper was financially supported by The Program for Professor of Special Appointment (Eastern Scholar) at Shanghai Institutions of Higher Learning, China (no. DF2009-01), the Innovation Program of Shanghai Municipal Education Commission, China (no. 10ZZ126), the International S&T Cooperation Project (contract no. 2007DFA50590) and the National High Technology Research and Development Program of China (863 Program) (contract no. 2009AA03Z230). The project was sponsored by the Scientific Research Foundation for the Returned Overseas Chinese Scholars, State Education Ministry, China. This work has received a support from the Norwegian Research Council.

References

[1] S. Orimo, H. Fujii, K. Ikeda, Acta Mater. 45 (1997) 331–341.
[2] K. Tanaka, J. Alloys Compd. 450 (2008) 432–439.
[3] Y. Wu, M.V. Lototsky, J.K. Solberg, V.A. Yartys, W. Han, S.X. Zhou, J. Alloys Compd. 477 (2009) 262–266.
[4] Y. Wu, W. Han, S.X. Zhou, M.V. Lototsky, J.K. Solberg, V.A. Yartys, J. Alloys Compd. 466 (2008) 176–181.
[5] Y. Wu, J.K. Solberg, V.A. Yartys, J. Alloys Compd. 446–447 (2007) 178–182.
[6] R.V. Denys, A.A. Poletaev, J.K. Solberg, B.P. Tarasov, V.A. Yartys, Acta Mater. 58 (7) (2010) 2510–2519.
[7] J.L. Bobet, B. Chevalier, M.Y. Song, B. Darriet, J. Etourneau, J. Alloys Compd. 336 (2002) 292–296.
[8] R.V. Denys, A.B. Riabov, J.P. Maehlen, M.V. Lototsky, J.K. Solberg, V.A. Yartys, Acta Mater. 57 (13) (2009) 3989–4000.
[9] B. Vigeholm, J. Kjølner, B. Larsen, J. Less-Common Met. 74 (1980) 341–350.
[10] R. Janot, F. Cuevas, M. Latroche, A. Percheron-Guégan, Intermetallics 14 (2006) 163–169.
[11] S.I. Yamaura, K. Isogai, H. Kimura, A. Inoue, J. Mater. Res. 17 (2002) 60–64.
[12] S. Yamamoto, Y. Fukai, E. Ronnebro, J. Chen, T. Sakai, J. Alloys Compd. 356–357 (356) (2003) 697–700.